Chapter 3

Designs of collector-chimney of PV integrated SCPP

This chapter examines the possibility of integrating a photovoltaic (PV) module in a hybrid solar chimney power plant (HSCPP). Since HSCPP is a greenhouse thermal buoyancy-driven system, the surrounding high temperature environment makes PV module temperature extremely high resulting in lower electrical conversion efficiency. Various design configurations of collector duct and solar chimney are investigated using an experimentally validated numerical model to study the PV panel cooling and turbine power output. The results show that turbine power output is sensitive to diverging the chimney up to maximum static pressure recovery limit while PV module shows marginal increase in electrical efficiency. Converging the collector duct alone shows worst turbine and PV module performance. However, in case of combine designs of converging duct and divergent chimney, considerable improvement of PV panel efficiency (about 7%) was observed. The results show that about 80% of the collector area measured from the chimney axis are the most effective region for cooling the PV module where consistent temperature drop of $10 - 12^{\circ}$ *C was observed. A design map vs. PV panel efficiency has been shown charting future directions for designing such energy efficient hybrid solar chimney systems.*

3.1 Introduction

Excessive environmental pollution by fossil fuels associated with high cost has driven researchers to replace it with efficient renewable energy based devices. Among renewable energy resources, solar energy is a vast source of heat and abundantly available during day time. The energy associated with the solar radiation received by the earth's surface is in the diluted form, unlike concentrated energy resources such as coal, petroleum, natural gas, etc. Hence, solar-thermal devices have large physical dimensions with larger surface area to harness maximum solar radiation for its operation. Solar chimney, electricity generation via photovoltaics, and solar air heaters etc. are some examples. Therefore higher input and maintenance costs are associated with these solar based energy systems. Researchers across the globe are developing various alternatives for environment-friendly power generation techniques to meet domestic and industrial energy demands. A device known as solar chimney is known for electric power generation has become a new research area among the scientific community. The device has some disadvantages in terms of high land procurement cost due to large ground area requirements, high initial cost, and low power output.

A typical solar chimney is a thermo-syphoning air channel device comprises of a circular/disc shape collector and a vertical chimney placed at the center of the collector [169, 71]. The collector comprises with a top transparent cover held horizontally at a small distance above the ground level which forms the flow channel for airflow. The solar radiation incident on the ground after passing through the transparent cover gets heated and generates high buoyancy forces [114, 110]. The updraft generated by the chimney guides the flow inside the collector to travel from the collector to chimney [110, 44]. A wind turbine is mounted at the collector outlet. The airflow in the collector drives the wind turbine to generate electric power ($P_{turbine}$) which is a function of cube of the airflow velocity at the collector outlet (V), $P_{turbine} \propto V^3$ [123, 26].

One way to increase the electricity output is by increasing the collector surface area which would enhance the buoyancy forces to increase the airflow velocity in the collector [82]. Output power can be further increased without increasing the solar collecting area if the solar chimney is integrated with a photovoltaic system.

Though there have been many studies on increasing the electricity output of a solar chimney [37, 136, 159], investigations on possibility of integrating a photovoltaic (PV) panel and its performance study in a variety of design configurations of a solar chimney is scarce. Most of the researchers integrated turbine in the solar chimney for enhancing the power output by changing the designs of solar chimney (see Table 3.1). It can be seen from the table that there are many design variables in the solar chimney design that effects its thermal performance such as collector area, height, slope and entrance slope; chimney height, radius and divergence; solar radiation, turbine pressure drop and its efficiency. Apart from these geometric optimisation, there have been many other studies where hybridisation of solar chimney power plant has been investigated. For example, apart from integrating a wind turbine [6], studies have been reported on integrating thermal storage [44, 21], waste heat recovery [7], space heating [6], desalination plant [6, 105], solar cyclone for harnessing atmospheric water [80] etc. An interesting analysis on integrating a solar cyclone in solar chimney was presented by [80] for the condensation and separation of water from the atmosphere. Their analysis suggested that a single solar cyclone 500 m high could satisfy the household fresh water needs, and about 75% of the electrical needs, for an urban population of 10,000 residing in an arid region. Evidently, hybridization of solar chimney power plant would pay off if hybridisation of other established technologies such as PV panel is investigated and system design is optimized.

One of the reason for scarce scientific literature on PV panel and solar chimney hybrid system is that PV panel electrical output is severely affected by the high temperature, greenhouse environment prevalent in the solar chimney [60]. For crystalline silicon photovoltaic cells, every 1 degree rise in temperature reduces the electrical efficiency of a PV panel by 0.2-0.5% [103]. Clearly, for PV panel to work efficiently in a solar chimney, its cooling mechanisms has to be properly devised. Many investigators have reported the effect of cooling the PV panel using air [60, 103], water [103], and phase change materials [103, 99]. When water is made to flow over the glass top surface of the panel, its efficiency increased by about 9% [103]. However, in systems like solar chimney, using water or other mechanisms for PV panel cooling would become cumbersome that may result into high maintenance cost. Therefore, the same fluid medium which is used for solar chimney operation seems to be the preferred choice. However, owing to its lower thermal conductivity, air can serve as cooling fluid if its velocity is increased significantly.

The objectives of this chapter are three-fold: first, explore the possibility of integrating a PV panel in a solar chimney and investigate all avenues for increasing its electrical efficiency by cooling the panel. Second, investigate designs parameters for trade-off between turbine and PV panel requirements. Turbine power output and PV panel electrical output comes at the each others expense. High cooling of PV panel would reduce the buoyancy force which is against the requirement of high turbine output. Most of the previous studies were carried out concentrating on thermo-hydraulic performance occurring inside the solar chimney. However, in practice, when a PV panel is integrated with the system, realistic modelling is necessary. Hence, the third objective is to evaluate such hybrid solar chimney system under more realistic conditions. All these objectives are met by strategizing appropriate design changes in the conventional solar chimney configurations. The turbine power output in terms of velocity gain and PV panel electrical efficiency in terms of its temperature drop were monitored. Since the efficiency of solar chimney is hardly 2% [6], authors hope that this chapter would provide insights and blueprint for various design strategies for enhancing the efficiency of such important solar power plant systems.

3.2 Hybrid solar chimney model description

Fig. 3.1 shows the new design description of the computational model of the hybrid solar chimney power plant (HSCPP) integrated with a PV panel. Other design configurations of hybrid solar chimney has been shown in Fig. 3.2. The HSCPP mainly comprises of a circular collector at the ground level placed horizontally with a tall vertical chimney installed at the centre. The collector consists of a transparent cover as upper surface and the PV module/solar cell as bottom surface making up the flow channel through which heated air flows

naturally under the buoyancy effect. The transparent cover allows short wavelength solar radiation to transmit through it and opaque to long-wavelength radiation emitted from the PV module. The ambient air enters from the collector inlet, flows over the high-temperature PV module and exit from the chimney outlet. The chimney basically guides the flow inside the collector by enhancing updraft and, hence, the flow driving potential. The various design parameters of solar chimney and PV module layer characteristics are provided in tables 3.2 and 3.3, respectively. Various designs of flow channel has been shown in Fig. 3.2.

Table 3.1 Literature on solar chimney (SC) investigations.

Authors	**System**	**Analysis area**	**Effective parameters and range**	**Findings**
[60]	Solar chimney + PV panel	• Collector channel • Optimum location for placement of PV panels	• Widths of PV panel = 70, 50, 30 cm	• Maximum PV panel electrical output achieved for 50 cm width optimum
[37]	Solar chimney	• Performance of divergent chimney	• Divergent angle, $\phi_{ch} = 1^{\circ} - 5^{\circ}$ • Solar flux, I=600-900 W/m^2	• Best,$\phi_{ch} = 1^{\circ} - 2^{\circ}$ • Maximum increase of 58% in the air velocity
[136]	Solar chimney	• Collector entrance gap (a) • Chimney diameter (b) • Chimney height (h) • Collector roof inclination (ϑ)	$0.1 \leq a \leq 0.2$ $0.2 \leq a \leq 0.2$ $8 \leq h \leq 16$ $0^{\circ} \leq \theta \leq 20^{\circ}$	Power output decreases with increase in 'a' and 'ϑ'; increases with increase in 'b' and 'h'.
[62]	Solar chimney	• Chimney divergence angle (β) • Collector slope (α)	$\beta = 1^{\circ} - 3^{\circ}$ $\alpha = 4^{\circ}, 6^{\circ}, 8^{\circ}, 10^{\circ}$	• Increasing α enhanced SC performance; deteriorates for higher α values. • Lower β values improved the SC performance.
[17]	Solar chimney	• Influence of collector inclination angle (β) on the solar chimney performance.	$\beta = 0^{o}\ to\ 1.5^{o}$	125% increase in flow velocity; Collector inclination angle has a positive impact on the SC performance.
[159]	Solar chimney + wind turbine	Thermal performance analysis with the parameters: • solar radiation • turbine pressure drop • turbine efficiency	• Solar radiation 200, 400, 600 and 800 W/m^2 • Turbine pressure drop 40, 120, 200, 280 Pa	• High solar radiation improves turbine efficiency. • Increasing pressure drop increases power output; performance deteriorates later.
[79]	Solar chimney	Solar chimney performance was evaluated for the range of collector entrance height (h) and chimney height (H).	• $h = 6 - 12cm$ • $H = 100 - 300cm$	The best SC performance with collector entrance with 6 cm, chimney height 300 cm, and chimney diameter 30 cm.
[52]	Solar chimney	• Collector height (h)	• $h = 4 - 14cm$	SC performance was found to be maximum for the lower value of collector height i.e. 6 cm.
[54]	Solar chimney + wind turbine	Examined the effect under variable: • solar heat flux • turbine pressure drop • ambient temperature	• Solar radiation = 200, 400, 600 and 800 W/m^2. • Ambient temperature = 287-307 K • Pressure drop = 0 to 480 Pa	• High ambient temperature decrease power output. • Solar flux and turbine pressure drop has a considerable effect on SC performance.

[55]	Solar chimney + wind turbine	Compared optimal turbine pressure drop ratio of solar chimney via: • theoretically • numerical approach • solar radiation	• Solar radiation = 200-1000 W/m^2 • Turbine pressure drop	• The optimal pressure ratio with varying solar radiation around 0.9 for the Spanish prototype.
[16]	Solar chimney	• Collector roof height (h)	•$h = 50 - 200mm$	Decreasing h increases the power output due to increase in the air velocity.
[160]	Solar chimney	• Chimney outlet-to-inlet area ratio (COAR) i.e. divergent chimney	• COAR = 1, 3.9, 8.7, 9.9, 11.9, 15.5, 24.2	Maximum power output of 231.7 kW was achieved at COAR =8.7 which was 11.9 times greater than conventional COAR=1.
[45]	Solar chimney	• Collector roughness impact	Roughness height (h), width (L) and pitch (e) in the range: • h = 0.1-0.6 m, • L = 0.1, 0.2, 0.3 m, • e = 9.7 m	• Air velocity decreases due roughness. • Heat transfer enhanced resulting in higher air temperature.
[86]	Solar chimney	• sloped collector • collector area A_r • system height h_c	• $Ar = 500,000 - 1,200,000m^2$ • $h_c = 500 - 1000m$	Efficiency increases with increase in the system height and collector area.
[107]	Solar chimney	• collector area • chimney diameter • chimney height	• Collector dia. $d = 20 - 220m$ • Chimney dia. $d = 0.5 - 9m$ • Chimney height $h = 12 - 187m$	For optimum dimensions of the solar chimney: • h and d should vary in proportion for better performance.
[124]	Solar chimney + wind turbine	Numerically studied 3D SC power plant; compared with and without pressure drop ΔP.	• ΔP=40-220 Pa • Interval 20 Pa	The volume flow rate of air decreases and turbine power output increases with increase in ΔP.

Table 3.2: Design parameters of solar chimney [52].

S. No.	Parameters	Values of parameters
1	Collector inlet, H_1	6 - 18 cm
2	Collector outlet, H_2	6 cm (fixed)
3	Collector radius, R	150 cm
4	Chimney height (fixed)	300 cm
5	Chimney inlet radius, R_{ci}	10 cm (fixed)
6	Chimney outlet to inlet radius ratio, (CORR= R_o/R_i)	1, 1.5, 2, 2.5, 3, 3.5, 4, 4.5, 5
7	Collector solar irradiance (W/m^2)	850
8	Air velocity at the air inlet section	Stagnation state

Figure 3.2 shows the design modifications that has been incorporated in the conventional design. The performance improvement of the HSCPP has been substantially enhanced by two ways: 1. Tapering the collector flow passage; 2. Divergent chimney by increasing cross-sectional area of the chimney outlet, i.e. defined by the

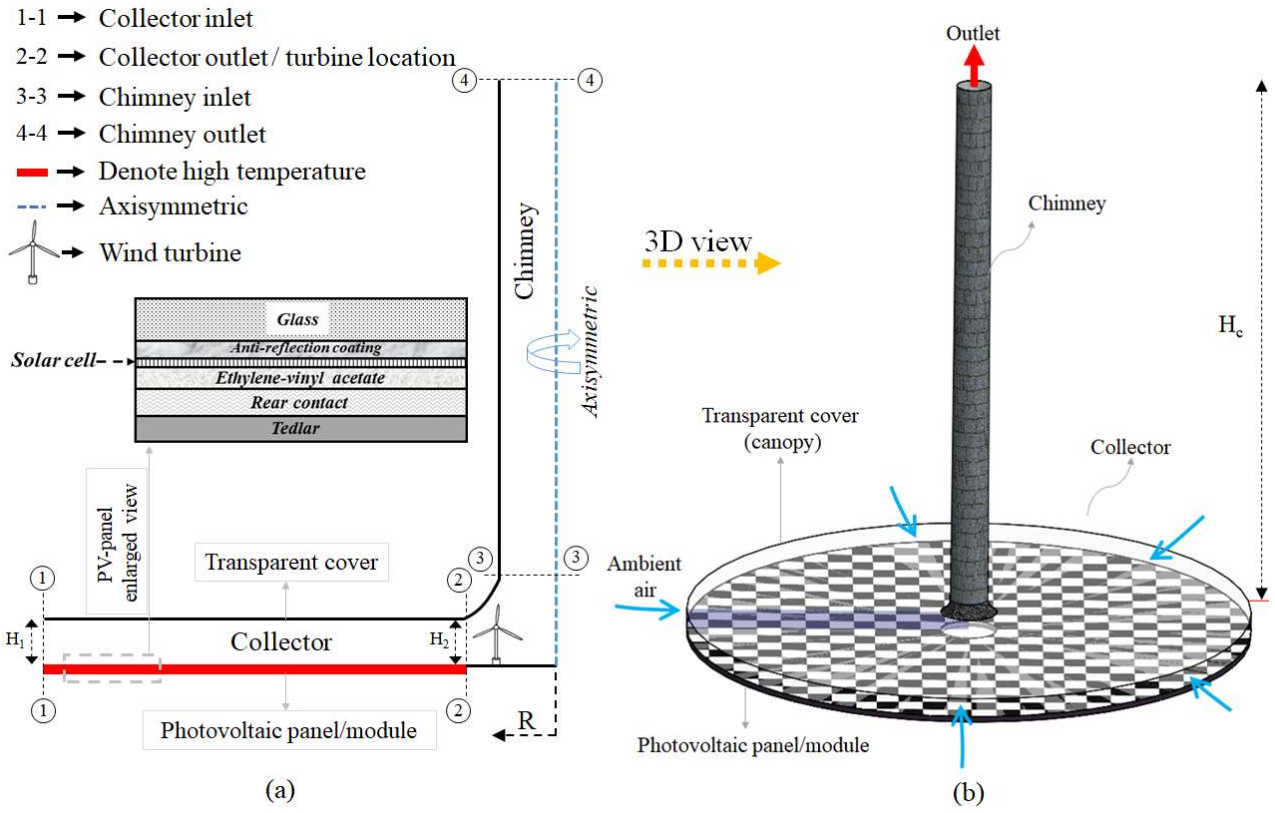

Figure 3.1: Schematic diagram of a new hybrid solar chimney power plant: (a) Two-dimensional axisymmetric model; (b) Three-dimensional view of computer aided design (CAD) model after 360° rotation. Enlarged view of the PV panel is shown as inset. Sections are marked with numbers where performance data is reported. Design changes in flow channel is shown in Fig. 2.

term chimney outlet to inlet radius ratio, CORR. Most importantly, there is a suitable combination of duct convergence and chimney divergence which gives best performance of PV and turbine power output.

Table 3.3: Polycrystalline silicon PV module characteristics [60].

S. No.	Layer	Thickness (m)	Density (kg/m^3)	Specific heat, C_P (J/kg°C)	Thermal conductivity (W/m.K)
1	Glass	0.003	3000	500	1.8
2	Anti-reflection coating	1×10^{-7}	2400	691	32
3	Mono-crystalline cell	2.25×10^{-4}	2330	677	148
4	Ethylene-vinyl acetate	5×10^{-4}	960	2090	0.35
5	Rear contact	1×10^{-5}	2700	900	237
6	Tedlar	0.0001	120	1250	0.2

3.3 Numerical domain: discretization and modelling

To analyze the performance of HSCPP, the computational domain has been discretized using finite volume method. The optimum grid size has been selected from the grid independent study. Structured boundary layer mesh was obtained with very fine layered mesh near the walls (refer Fig. 3.3) for accurate flow and heat transfer predictions near the heated surfaces. Near walls dimensionless wall distance (y^+) was kept less than unity. Mesh generation and simulation analysis has been conducted using Altair HyperWorks software.

3.3.1 Boundary conditions

Two-dimensional, steady-state and axisymmetric numerical simulation of hybrid solar chimney has been developed [110, 55, 107]. The chimney middle axis of the 2D computational domain was assigned as axisymmetric

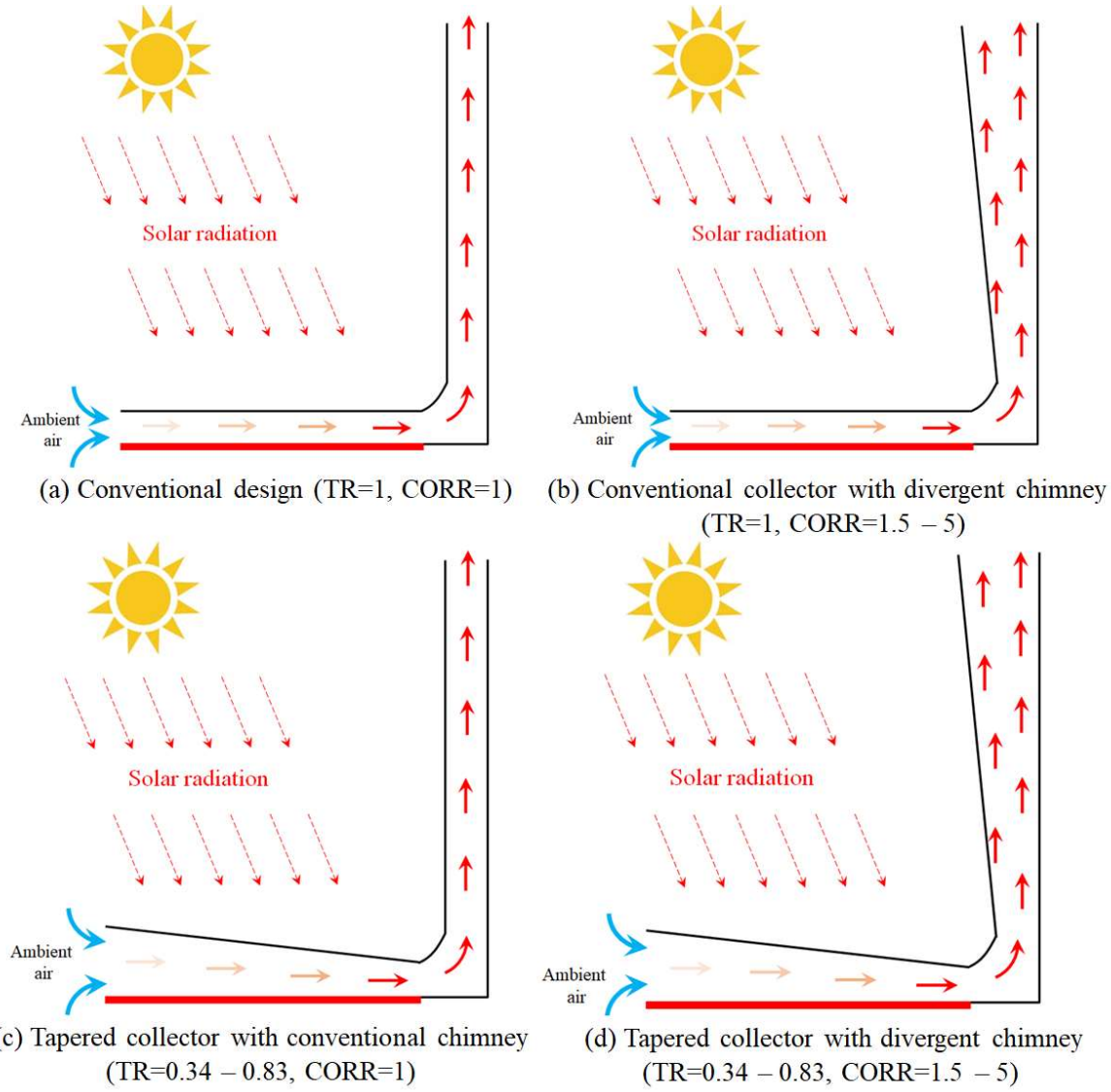

Figure 3.2: New designs of the hybrid solar chimney power plant with range of taper ratio $TR = 0.34 - 0.83$ and $CORR = 1 - 5$. (a) Conventional design; (b) Conventional collector with divergent chimney; (c) Tapered collector with conventional chimney; (d) Tapered collector with divergent chimney.

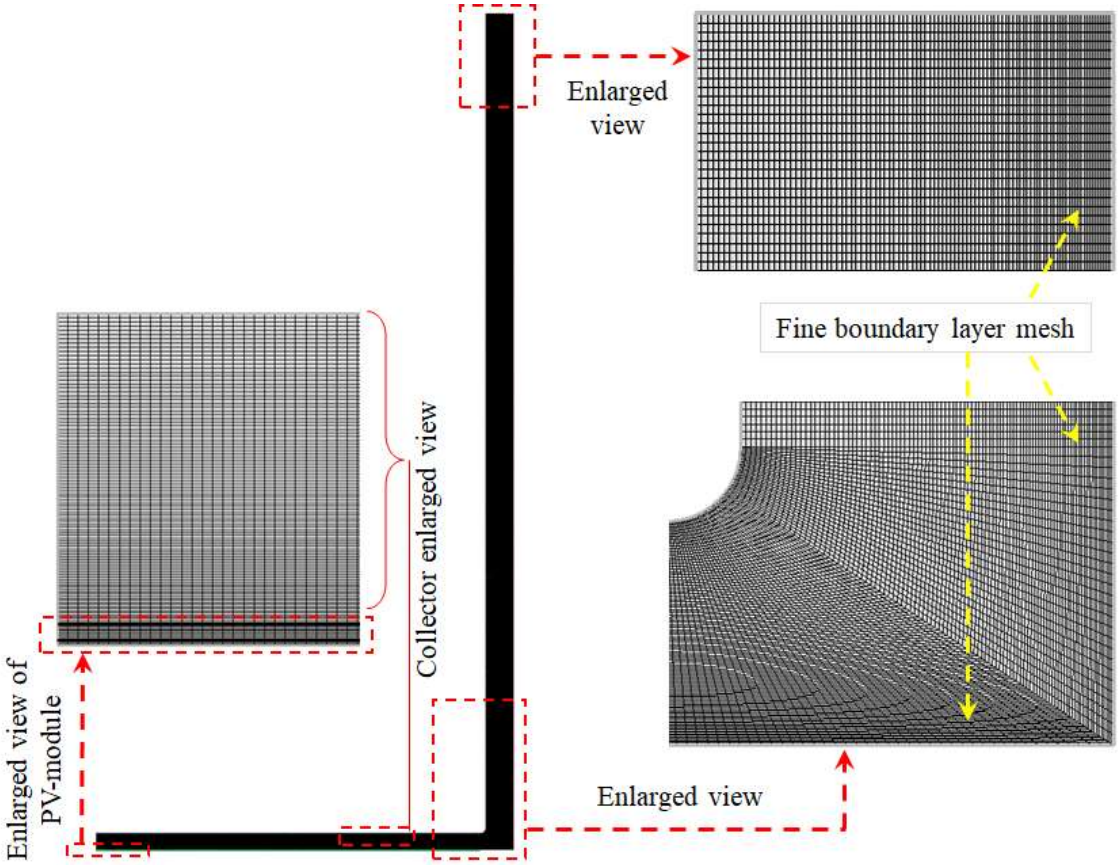

Figure 3.3: Meshed computational domain of HSCPP design with enlarged view of different zones.

to obtain results identical to 3D. This saves the computational time and resources. The collector inlet was at ambient condition, i.e. total pressure is equal to zero which is similar to the stagnation state assuming standstill environmental wind condition.

The chimney outlet was assigned pressure outlet condition where pressure equals atmospheric pressure (i.e. $P_{gauge} = 0$). The collector exposed to solar irradiance of 850 W/m^2. The top transparent cover of the collector was assigned convection heat transfer coefficient of 5.7 W/m^2 as per correlation $h = 5.7 + 3.8V_\infty$ (W/m^{2}K) [150], where V_∞ denotes environmental wind velocity, which is taken here as zero assuming standstill condition. In standstill ambient conditions, the equivalent convection heat transfer is identical to radiation heat transfer coefficient [150]. To simulate practical conditions, the discrete ordinate (DO) radiation model has been considered in the numerical simulations [54, 55, 110]. The DO model is the only radiation model that detect non-gray radiation using gray band model and works efficiently for the entire range of optical thickness [54]. The walls of the domain have been assigned no-slip condition. The Boussinesq model was considered to take care of the density variation with temperature gradient in the buoyancy term (refer Eq. 3.1) of the momentum equation [110, 54].

$$(\rho - \rho_\infty)\, g = -\rho_\infty \beta\, (T - T_\infty)\ \ g \tag{3.1}$$

where ρ_∞ is the density of the fluid at ambient condition, T_∞ is the temperature of the fluid at ambient condition, and β is the thermal expansion coefficient. The Boussinesq approximation is valid in case of the solar chimney as the product $\beta\,(T - T_\infty)$ is significantly less than unity [110].

The polycrystalline silicon photovoltaic panels has a top glass layer and rest layers are modelled considering equivalent properties listed in Table 3.3. The conjugate heat transfer occurs between array of PV modules at the ground and the fluid flowing inside the collector flow passage.

Details of photovoltaic characteristics are listed in Table 3.3.

A list of various boundary conditions at various sections is provided below in Table 3.4.

The thermo-physical properties of ambient air at the collector inlet are listed in Table 3.5.

Table 3.4: Boundary conditions

S. No.	Location	Description
1	Collector inlet	$P_{total} = 0\,Pa$, $T_\infty = 298\,K$
2	Collector solar irradiance, W/m^2	850
3	Chimney outlet	$P_{gauge} = 0$ (atmospheric condition)
4	Chimney walls	Heat flux, $q = 0$ W/m^2 Adiabatic
5	Convection heat transfer coefficient of the top glass plate was determined by $h = 5.7 + 3.8V_\infty$(W/m^{2}K)	5.7 (for standstill atmosphere $V_\infty = 0$) [31]

Table 3.5: Ambient fluid properties at the collector inlet of HSCPP at ambient temperature of 300 K.

Properties name	Value
Dynamic viscosity (μ)	1.855 x 10^{-5} Ns/m^2
Thermal conductivity (k)	0.026 W/m K
Prandtl number (Pr)	0.71
Specific heat (C_P)	1003.62 J/kg K
Density (ρ)	1.184 kg/m^3

The flow inside the solar chimney is fully turbulent in nature. The standard $k-\varepsilon$ model has been used [110, 107, 124]. The results obtained using standard $k-\varepsilon$ model predicts close values with the experimental data of the literature [52]. The primary governing equations considered in the model are mentioned below [71, 16],

Continuity equation,

$$\frac{\partial}{\partial x}(\rho u) + \frac{1}{r}\frac{\partial}{\partial r}(r\rho v) = 0 \tag{3.2}$$

Momentum equations,

$$\frac{\partial}{\partial x}(\rho uv) + \frac{1}{r}\frac{\partial}{\partial r}(r\rho vv) = -\frac{dp}{dr} + \frac{1}{r}\frac{\partial}{\partial r}\left[(\mu+\mu_t)\,r\frac{\partial v}{\partial r}\right] + \frac{\partial}{\partial x}\left[(\mu+\mu_t)\left(\frac{\partial v}{\partial x}+\frac{\partial u}{\partial r}\right) - 2(\mu+\mu_t)\frac{v}{r^2}\right] \tag{3.3}$$

$$\frac{\partial}{\partial x}(\rho uu) + \frac{1}{r}\frac{\partial}{\partial r}(r\rho uv) = -\frac{dp}{dx} + \frac{1}{r}\frac{\partial}{\partial r}\left[(\mu+\mu_t)\,r\left(\frac{\partial u}{\partial x}+\frac{\partial v}{\partial r}\right)\right] + 2\frac{\partial}{\partial x}\left[(\mu+\mu_t)\frac{\partial u}{\partial x}\right] + \rho_o\beta g\,(T-T_o) \tag{3.4}$$

Energy equation,

$$\frac{\partial}{\partial x}(\rho uT) + \frac{1}{r}\frac{\partial}{\partial r}(r\rho vT) = \frac{1}{r}\frac{\partial}{\partial r}\left[\left(\frac{\mu}{Pr}+\frac{\mu_t}{\sigma_t}\right)r\frac{\partial T}{\partial r}\right] + \frac{\partial}{\partial x}\left[\left(\frac{\mu}{Pr}+\frac{\mu_t}{\sigma_t}\right)\frac{\partial T}{\partial x}\right] \tag{3.5}$$

For the standard $k-\varepsilon$ model, the equations for turbulent kinetic energy k and dissipation rate of turbulent kinetic energy ε are written as;

$$\frac{1}{r}\frac{\partial}{\partial r}(r\rho vk) + \frac{\partial}{\partial x}(\rho uk) = \frac{1}{r}\frac{\partial}{\partial r}\left[r\left(\mu+\frac{\mu_t}{\sigma_k}\right)\frac{\partial k}{\partial r}\right] + \frac{\partial}{\partial z}\left[\left(\mu+\frac{\mu_t}{\sigma_k}\right)\frac{\partial k}{\partial z}\right] + G_k + \beta g\frac{\mu_t}{\mathrm{Pr}_{kt}}\frac{\partial k}{\partial z} - \rho\varepsilon \tag{3.6}$$

$$\frac{1}{r}\frac{\partial}{\partial r}(r\rho u\varepsilon) + \frac{\partial}{\partial x}(\rho u\varepsilon) = \frac{1}{r}\frac{\partial}{\partial r}\left[r\left(\mu+\frac{\mu_t}{\sigma_\varepsilon}\right)\frac{\partial \varepsilon}{\partial r}\right] + \frac{\partial}{\partial x}\left[\left(\mu+\frac{\mu_t}{\sigma_\varepsilon}\right)\frac{\partial \varepsilon}{\partial x}\right] + G_k C_{1\varepsilon}\left(\frac{\varepsilon}{k}\right) - C_{2\varepsilon}\rho\frac{\varepsilon^2}{k} \tag{3.7}$$

where the constants values in the standard k- ε model are taken as $\sigma_k = 1$, $\sigma_\varepsilon = 1.3$, $C_{1\varepsilon} = 1.44$, $C_{2\varepsilon} = 1.92$. The SIMPLE (semi-implicit method for pressure linked equation) algorithm was used to resolve flow field

velocity and pressure of the computational domain.

3.3.2 Grid independence test

For the selection of optimum number of grids, a grid independence test was conducted considering the computational model of conventional solar chimney which was dimensionally identical to the experimental model [52]. The size and shape of the grid selected in such a way to obtain set convergence in optimum time and resources. Structured mesh generated to discretize the computational domain using quad shape element. Very fine boundary layer mesh generated near boundary walls for better captivity of flow. The numerical simulations were performed for various grid sizes and corresponding variation in the flow velocity along the collector radii was obtained. The test was conducted for four different number of elements are: 92980, 114600, 159400 and 225820, all the cases were simulated numerically under the same sets of boundary conditions. Figure 3.4 shows the variation of the flow velocity along the collector radii. Almost identical trend is observed for all the cases, and due to insignificant variation the number of elements, 114600 grids has been selected to carry out further simulations.

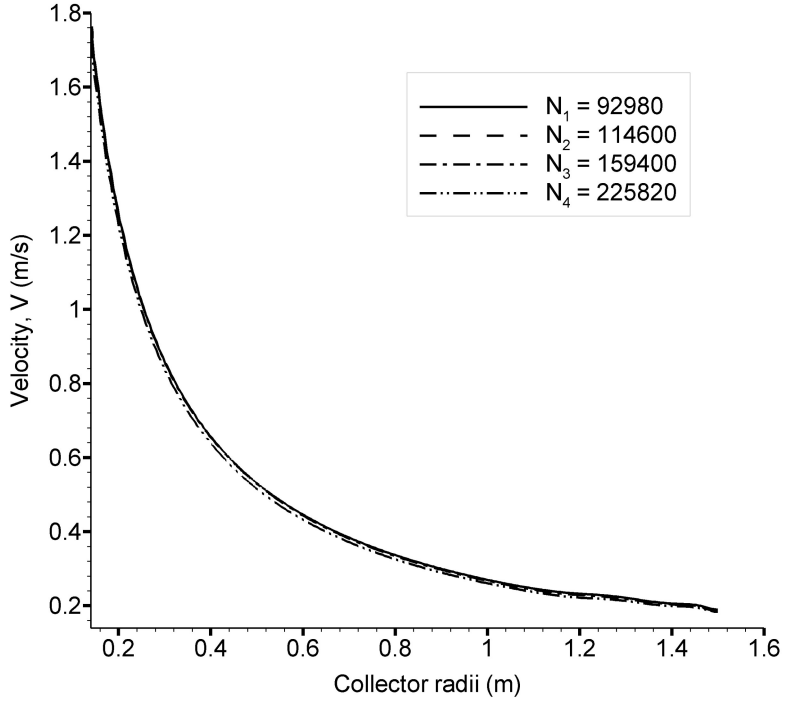

Figure 3.4: Grid independence test for different number of elements shown for the conventional design of solar chimney having dimensions identical to the experimental design of the literature [52].

3.3.3 Experimental setup and validation

To check the authenticity of the numerical model, the data obtained by simulations have been compared with the experimental data of the literature [52]. The model dimensions identical to the experimental setup of Ghalamchi et al., 2016 [52] (see Fig. 3.5(a)) was developed. Dimensions are listed in table 3.2. The boundary conditions as discussed above was applied. Since they reported the results for solar irradiance of 850 W/m^2, same heat flux was in our model.

Figures 3.5 (b) and (c) shows the velocity and temperature profile, respectively, along the collector radii. It can be seen that model predicts the trend in velocity and temperature variation similar to the experimental data. However, model prediction is consistently higher across the length. About 4-5% higher prediction in temperature from the model is seen near the inlet. Higher prediction can be attributed due to the following

reasons: First, we assumed that entire solar irradiance is received by the collector while the actual heat flux received by the collector in the experiments is generally a fraction less due to refraction and reflection from the surfaces and, and second, ambient velocity has some magnitude in experiments contrary to our standstill assumptions. Atmospheric wind contributes to higher heat losses from the system [159]. Third, mounting and fitting in experiments offers resistance to flow while all these losses are absent in the model. Therefore, due to perfect nature of the numerical model, its predictions are a bit higher. Nonetheless, the difference is within the acceptable limit and we can say that the model mimics the experimental conditions.

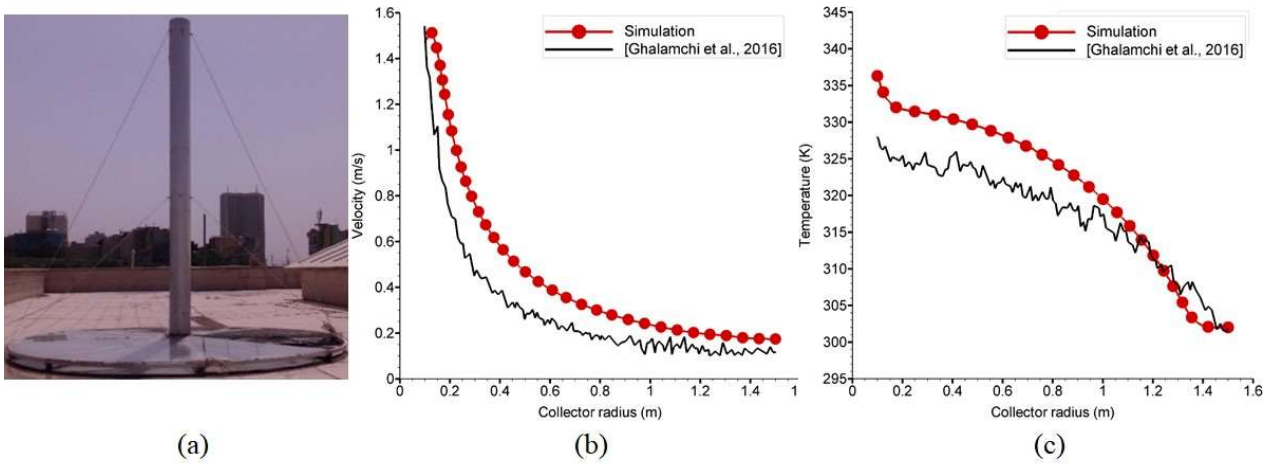

Figure 3.5: (a) Solar chimney experimental set-up [18]. Comparison of (b) velocity and (c) temperature profile obtained from numerical model with the experimental data of the literature [52].

3.4 Results and discussions

This article explores the possibility of integrating a PV panel inside the extreme greenhouse environment of a solar chimney with an aim to increase the electrical conversion efficiency of the panel. With rising population, energy demand is going to increase exponentially. To sustain the future with ever growing energy needs, avenues for increasing the efficiency of the hybrid solar chimney system is one step in this direction. Fortunately, most of the underdeveloped regions of the Earth are rich in sunshine. Such hybrid technology would be very much useful in making people's life more convenient if growing power needs are met. Most of the solar energy is converted into heat by the PV panel thereby reducing its electrical conversion efficiency [60, 43]. The atmospheric draft created inside the collector and channeled through the chimney holds the key. Suitable design changes in collector and chimney are investigated that aid in turbine and panel performance.

As stated earlier, the two-fold objective of this chapter is to increase the flow velocity for higher turbine power output and reduce the temperature of the PV panel. In a natural convection scenario for a given fluid, these objectives can only be achieved by suitably changing the design of the system. In this section, effect of design changes on dynamic performance of the hybrid solar chimney has been described by analysing flow behaviour and its thermal characteristics. The flow velocity, pressure and temperature variation in the entire flow domain are the major influencing factors and have been closely monitored.

The available power or the power generated by the turbine is expressed [123, 26, 62] as:

$$P_{turbine} = \frac{1}{2}\rho A V^3 \tag{3.8}$$

The efficiency of the photovoltaic is a function of temperature gradient $(T_c - T_r)$, where T_c and T_r are the temperature of the solar cell and reference, respectively. The PV panel efficiency expression is given as;

$$\eta = \eta_r \left[1 - \beta_r \left(T_c - T_r\right)\right] \tag{3.9}$$

The reference temperature $T_r = 25°C$, $\beta_r = 0.004081/K$ and reference efficiency $\eta_r = 15\%$ [43].

3.4.1 Effect of divergent solar chimney

The chimney is a vertical upward tower whose inlet is situated at the center of the collector to generate the optimum magnitude of air updraft to guide the airflow movement through the collector, which has cylindrical shape in case of conventional HSCPP design (see Fig. 3.2(a)). The above chimney design has been transformed into divergent shape with gradual increase in cross-section area at the chimney outlet/top while the bottom cross- sectional area is kept constant (see Fig. 3.2(b)). The performance of the HSCPP at various CORR has been examined and reported.

Figure 3.6 shows velocity along the collector radius for different CORR in the range 1-5 of divergent chimney. Ambient air enters from the collector inlet where flow interact with the high-temperature PV module placed at the ground. The heated air has tendency to flow along the collector radii due to buoyancy and updraft generated by the chimney. As the CORR of the divergent chimney increases, the flow velocity at the collector outlet first increases with increasing CORR value upto 3 and decreases afterward for higher CORR values. The maximum flow velocity 3.65 m/s was observed for CORR=3 which is 121.21% higher than the conventional cylindrical chimney i.e. CORR=1. This corresponds to about 363% increase in turbine power generation compared to the conventional design.

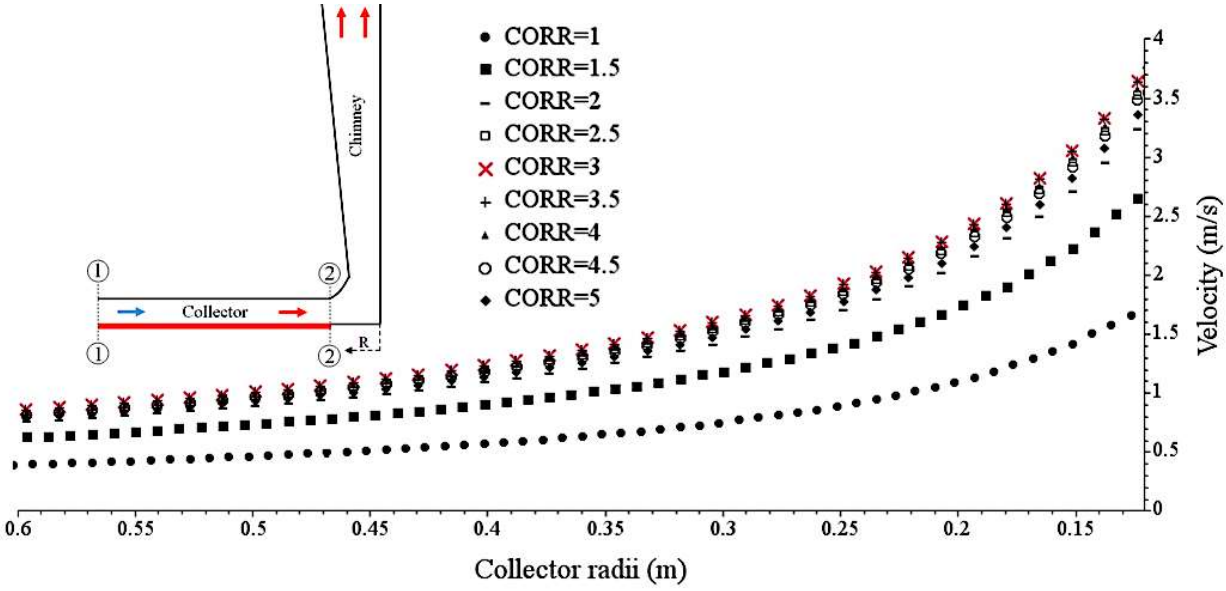

Figure 3.6: Velocity profile along the collector radius for different CORR values of divergent chimney. Variation is shown between 0-0.6 m where significant difference is seen. Zero radii is located at the center of chimney. CORR =1 corresponds to conventional chimney.

The increase in the flow velocity results in considerable drop in PV panel temperature, which results in enhancement of the PV panel efficiency as shown in Fig. 3.7. The efficiency increased by 4.4% compared to conventional design. The effective cooling of PV panel observed in the region near to the collector outlet or after small distance from the collector inlet.

The function of the chimney is to generate updraft in order to guide the fluid flow movement in the collector. The flow behavior in the divergent chimney is different from the conventional chimney design. Along the chimney height, the y-direction momentum equation is given as,

$$\frac{dp}{\rho g} + \frac{v\,dv}{g} + dz = C \tag{3.10}$$

where C is constant.

At the collector inlet, the pressure is equal to atmospheric pressure $P_{0\infty}$. The flow velocity gradually increases from inlet of the collector up to collector outlet. Meanwhile, the static pressure at the chimney inlet decreases below atmospheric due to the increase in dynamic pressure $\left(\frac{1}{2}\rho v_1^2\right)$ which is equal to $P_{0\infty} - \frac{1}{2}\rho v_1^2$, where v_1 is the air velocity at the chimney inlet. The static pressure at the chimney outlet is $P_{0\infty} - \rho_\infty g H$, where H is the chimney height.

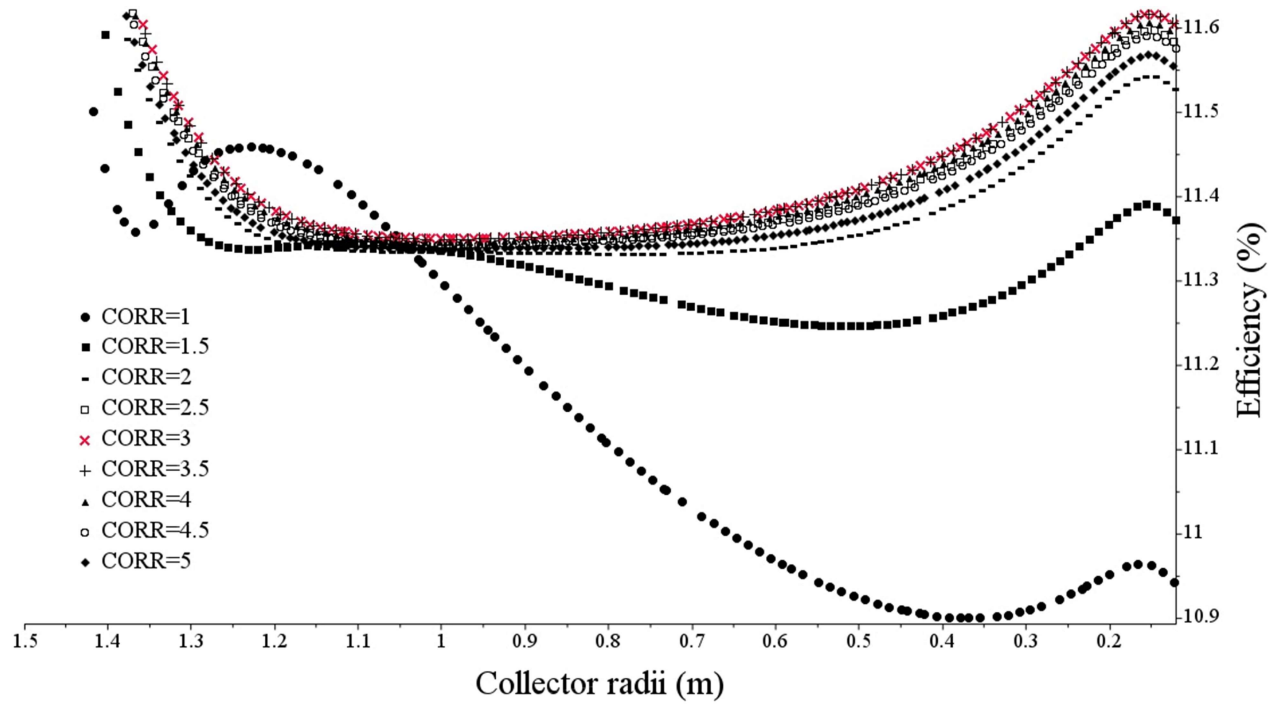

Figure 3.7: Local variation of PV panel efficiency along the collector radius for different CORR range 1-5 of divergent chimney. CORR =1 corresponds to conventional HSCPP.

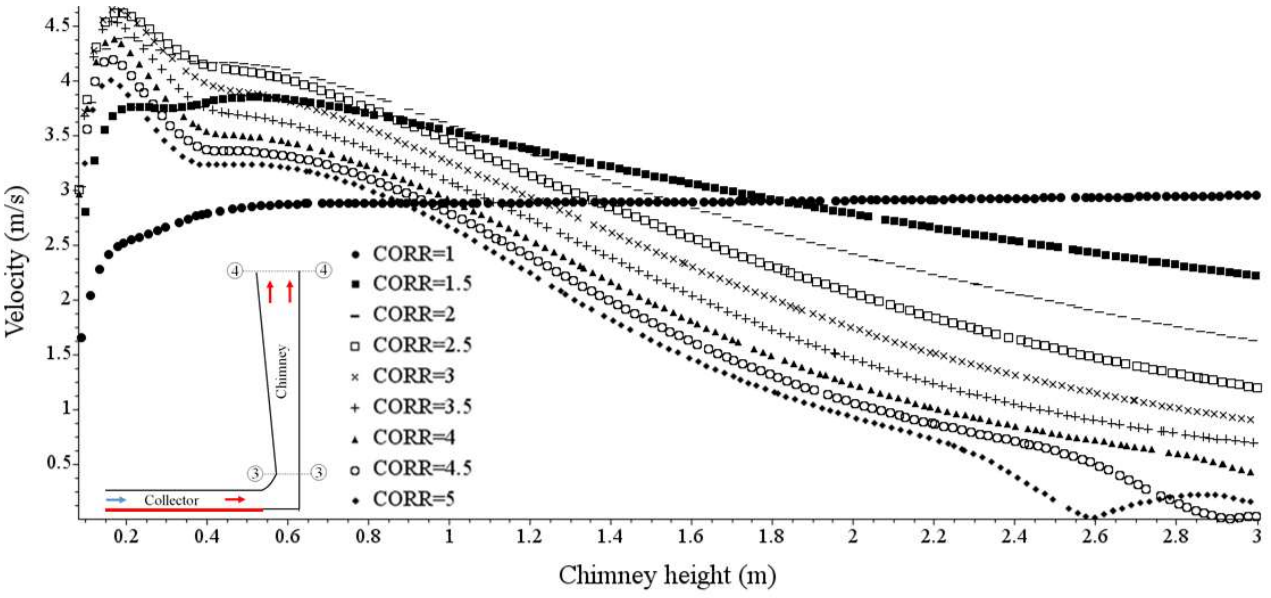

Figure 3.8: Velocity variation along the height of the chimney for different CORR range 1-5 of divergent chimney. CORR =1 denote conventional HSCPP.

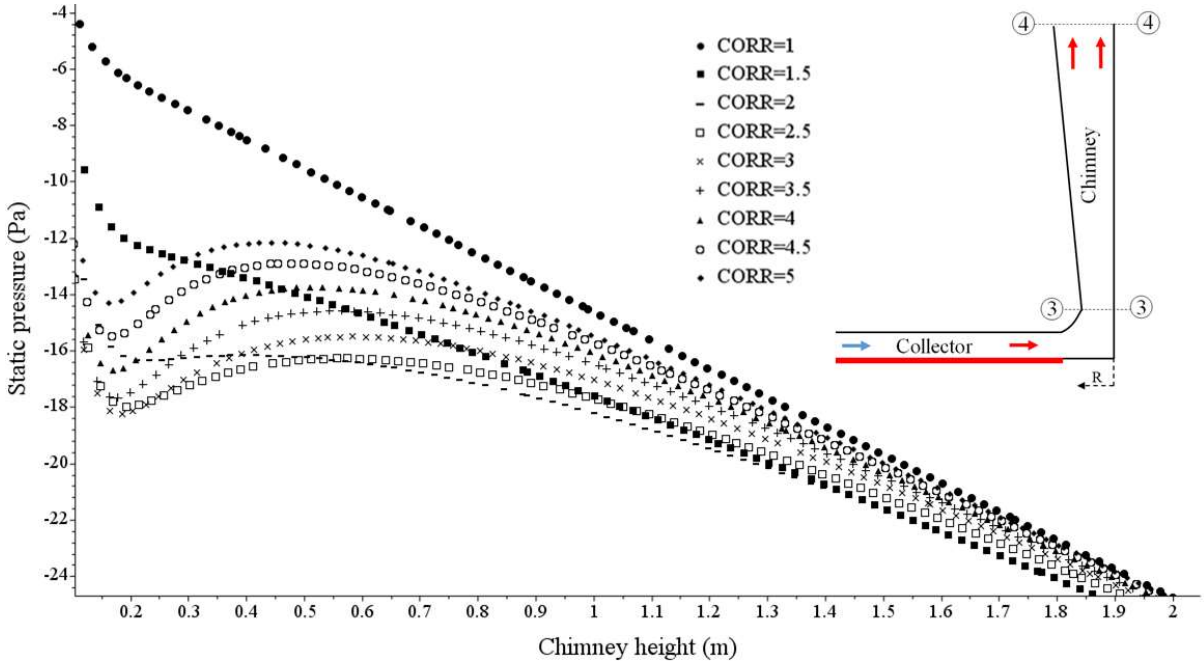

Figure 3.9: Static pressure variation along the height of the chimney for different CORR range 1-5 of divergent chimney. CORR =1 denote conventional HSCPP.

Figure 3.8 demonstrates the velocity variation along the chimney height of the HSCPP for different CORR values and the corresponding pressure variation is shown in Fig. 3.9. In case of conventional cylindrical chimney, the flow velocity almost remains constant. Meanwhile, increasing CORR value has a considerable impact over the flow field due to change in the pressure field. Increasing CORR value increases the velocity at the collector outlet and afterward decreases from chimney inlet to outlet due to static pressure recovery. The combined effect adds to the advantage in terms of improvement in the total pressure potential (TPP) (see Eq. 3.11) of the divergent chimney and hence the turbine power output. The increased flow velocity in the collector due to divergent chimney improves convection heat transfer rate from the PV panel which prevents it from overheating. The TPP expression has a functional relationship with the flow velocity at the chimney inlet and outlet and it is expressed as [62, 160];

$$TPP = \frac{1}{2}\rho\left(v_1^2 - v_2^2\right) + \left(\rho_\infty - \rho\right) gH \tag{3.11}$$

For conventional design the velocity at the chimney inlet and outlet are almost the same, and hence only the first term of Eq. 3.11 generates TPP. When compared with the conventional design, among all the divergent chimney cases, the CORR=3 attains the maximum flow velocity at the collector outlet, which shows an enhancement of 121.21% . However, velocity at the chimney outlet has been reduced by 58.33% . As discussed above, diverging the chimney shows significant improvement in the flow velocity resulting in the turbine power output. The increased flow velocity significantly enhances the heat transfer rate at the PV panel of HSCPP and increases its electric output efficiency by 4.4%.

Figure 3.9 shows the static pressure variation along chimney height. Significant pressure variation in the flow field has been observed at the inlet of divergent chimney. Divergent chimney showed adverse pressure gradient along the chimney height [71]. With increase in CORR value, the boundary layer separation promotes eddies formation near to the chimney wall and, hence reduced the flow area at the outlet. In Fig. 3.6, the maximum velocity at the collector outlet marked for $CORR = 3$, and the corresponding value of static pressure is -18.5 Pa. $CORR$ range $1.5 - 3$ has a positive impact on the overall performance of HSCPP as it increases the flow driving potential [62]. This noticeable increase in the TPP is responsible for the enhancement in the flow velocity at the collector outlet [71] and also the heat transfer rate from the PV panel, which increases electrical output efficiency (refer Fig. 3.7). Increasing CORR value from $3.5 - 5$ shows higher losses due to backflow and recirculating flows near to the chimney outlet section, which deteriorates the system performance.

Figure 3.10 shows velocity variation at the chimney outlet for the CORR range $1 - 5$. In conventional design

i.e. CORR = 1, velocity at chimney outlet is nearly equal to the velocity at the chimney outlet due to equal cross-sectional area and thus, the first term in the Eq. 3.11: $\frac{1}{2}\rho\left(v_1^2 - v_2^2\right)$ becomes negligible. This lead to negligible static pressure recovery along the chimney height. However, in divergent chimney cases the increasing CORR results in reduction of the velocity at the chimney outlet due to static pressure recovery. This is due to the existence of local adverse pressure gradient near the chimney exit generated in the region where boundary layer separates [71, 160]. Eddies formation at the chimney exit denotes higher loss in the flow. It is evident from the velocity line contours shown as inset in the figure. For CORR = 5, the recirculating flow forms positive and negative pressure regions. As vortex forms, the effective flow area at the chimney outlet reduces. Occurrence of backflow raised the possibility of mixing of cold surrounding air with the warm upcoming air [71]. This mixing reduced the buoyancy effect and hence, the flow velocity. Thus, total pressure at the outlet decreases to a minimum for CORR = 5 (see Fig. 3.11). For lower CORR, the flow enters the chimney inlet and exit without separation or stall formation.

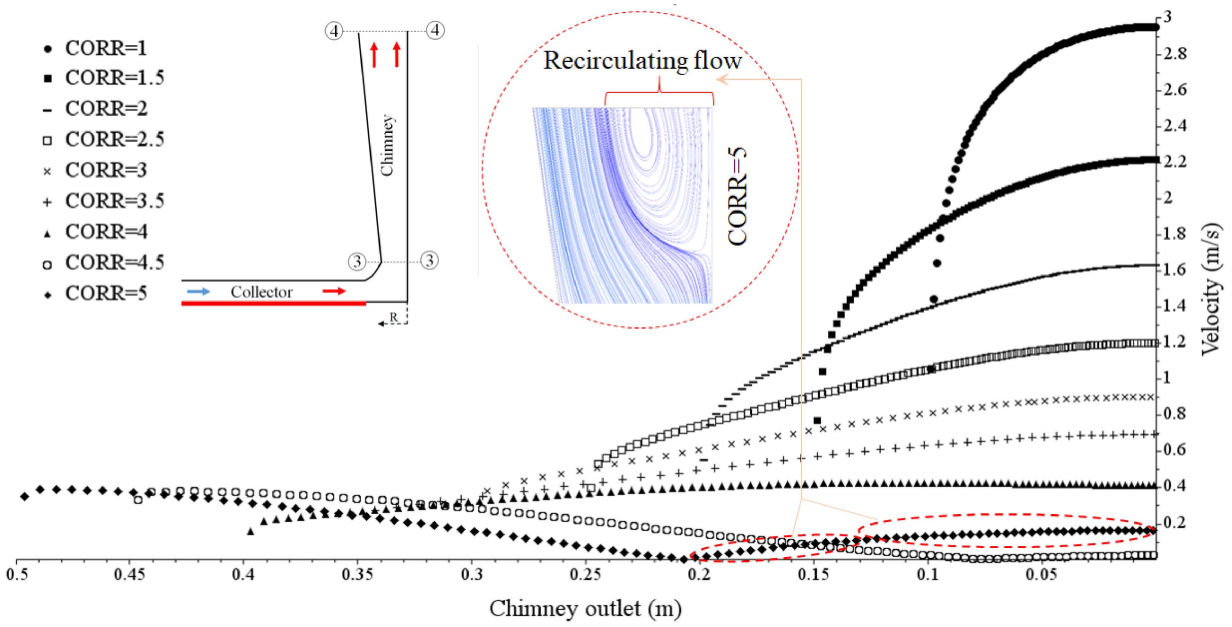

Figure 3.10: Velocity variation at the chimney outlet i.e. at section 4-4 for different CORR range 1-5 of the divergent chimney. At higher CORR, reverse flow is seen (see inset). CORR =1 denote conventional HSCPP.

3.4.2 Converging collector passage with divergent chimney

In conventional collector design of the solar chimney flow passage comprises the top transparent cover arranged parallel to the ground (Fig. 3.2(a)). In the present analysis, the transparent cover is inclined to horizontally placed PV panel at the ground, and the collector flow passage appears as taper flow passage. The term taper ratio, TR is the ratio of the collector opening height at the outlet H_2 to the inlet H_1. The collector opening height H_2 has been kept constant and $H_1$is made variable.

To increase the heat transfer rate from the PV panel two different design strategies were adopted 1. taper flow passage of collector with conventional cylindrical chimney (see Fig. 3.2(c)); 2. taper flow passage with divergent chimney (Fig. 3.2(d)).

Figure 3.12 shows the velocity profiles along the collector radii for TR range $0.34 - 1.0$ for conventional cylindrical chimney and divergent chimney. The transformation of parallel flow passage of the conventional HSCPP into taper flow passage boost the electrical output efficiency of PV panel by 4.5% as shown in Fig. 3.13. The cooling of the PV panel is high near to collector inlet, decreases at the midsection and then increases again as the flow marched along the collector radius towards collector outlet. This is an interesting observation. Due to high temperature difference between PV panel and fresh ambient air, PV panel experiences high heat transfer. As the air gains temperature due to greenhouse effect, PV panel efficiency slightly decreases but again increases near the exit due to higher flow velocity. Only tapering the collector flow passage has shown high

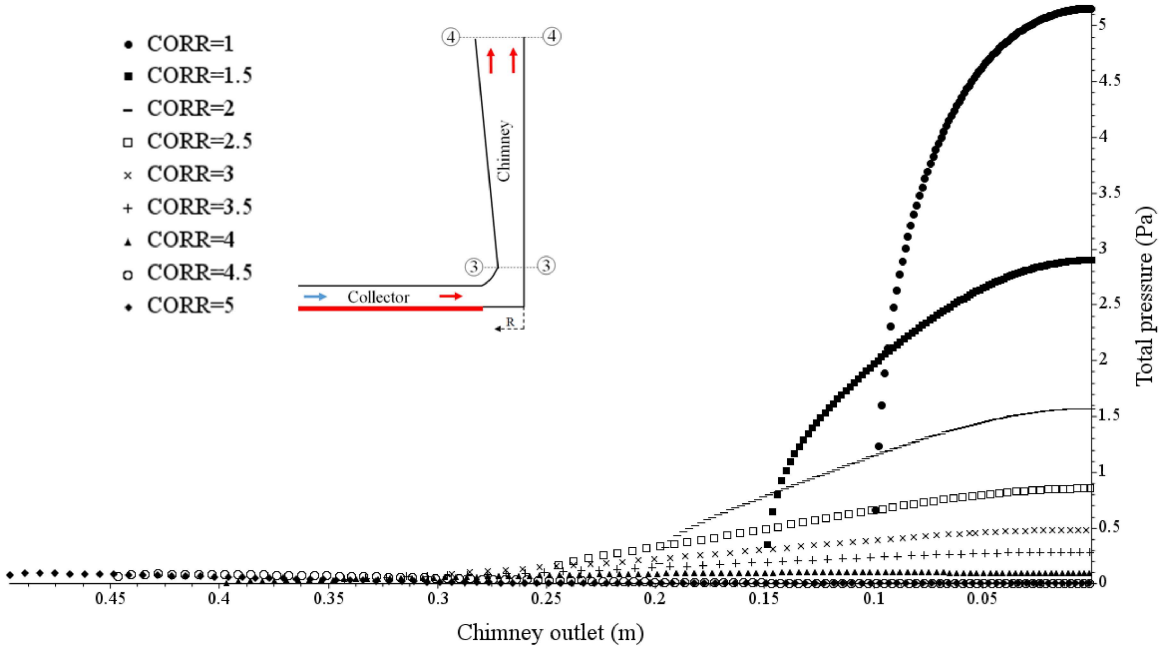

Figure 3.11: Total pressure variation at the chimney outlet i.e. section 4-4 for different CORR range 1-5 of divergent chimney.

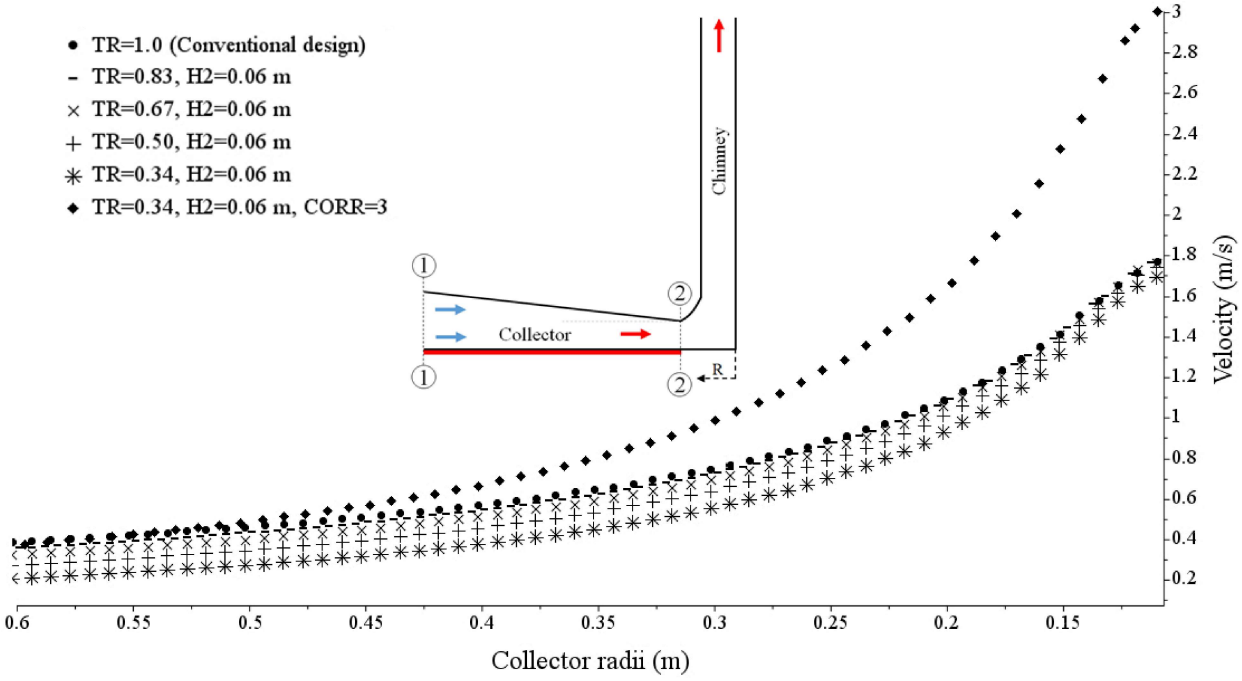

Figure 3.12: Velocity variation along the collector radii for different taper ratio (TR) range 0.34-1 with conventional cylindrical and divergent chimney. In all cases, the opening inlet height H_2 has been kept constant.

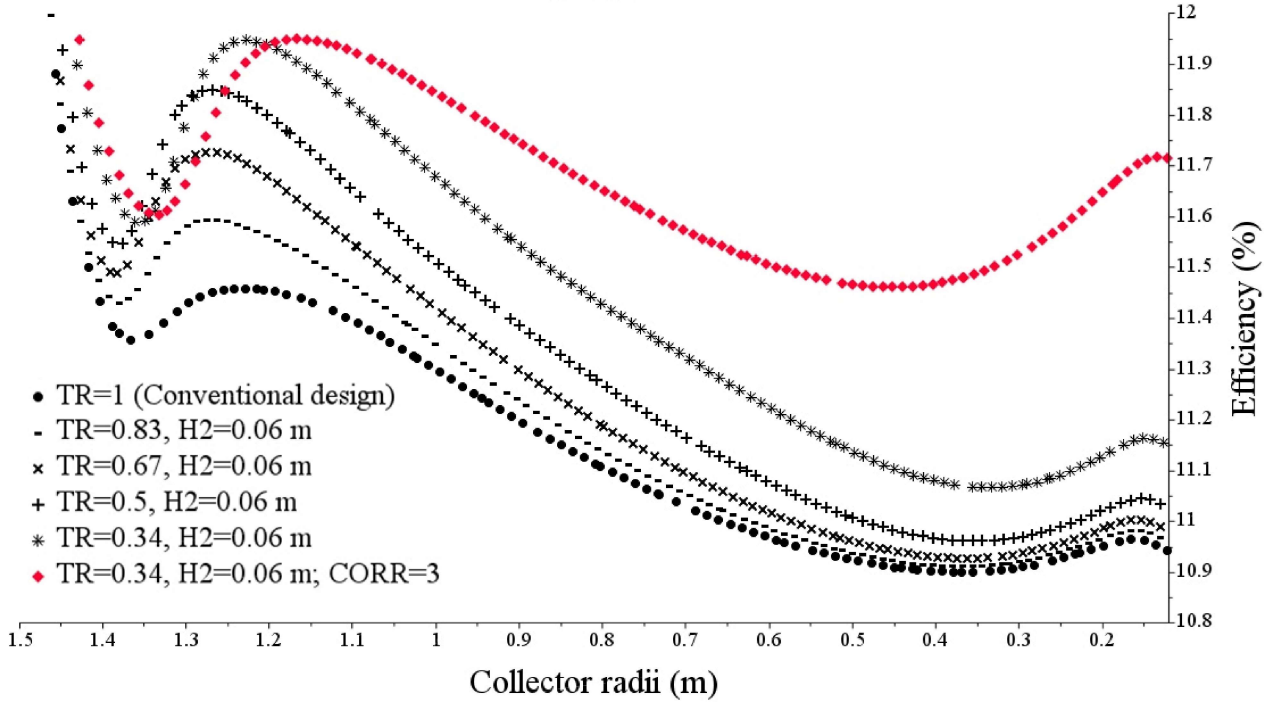

Figure 3.13: Efficiency variation of the PV panel along the collector radii for different taper ratio (TR) range 0.34-1 combined with divergent chimney.

impact on reducing the PV panel temperature. The collector having TR = 0.34 shows temperature drop of $3-8°C$.

As observed above, the best taper ratio was found to be $TR = 0.34$ and best $CORR = 3$. Now, we report the results of combing the tapered collector with divergent solar chimney. Substantial improvement in the magnitude of flow velocity at the collector outlet and significant drop in PV panel temperature was observed compared to the conventional design. The maximum percentage increase of 71.42% in the flow velocity and $8-12°C$ drop in the solar cell temperature was recorded, which enhances the efficiency of PV panel by 7% compared to conventional design (see Figs. (3.12 & 3.13) and Table 3.6). About 80% i.e. A = 0.8 R^2 of the collector area from the chimney axis that is $R = 0.1\,to\,1.2\,m$ shows consistent drop of $10-12°C$. PV panels can be placed in this 80% areas for better thermal and hence, electrical performance. This high temperature drop increases the PV output efficiency by about 7% . The turbine power output, $P_{turbine}$ increased by about 214% due to significant increase in flow velocity ($P_{turbine} \propto V^3$) at the collector outlet. The combination of taper collector and divergent chimney shows significant improvement in electrical performance of PV panel and turbine power output.

Figure 3.14 shows velocity inside the flow passage for various designs of HSCPP: (a)$TR = 1$, $CORR = 1$ (conventional); (b) $TR = 1$, $CORR = 3$; (c) $TR = 0.34$, $CORR = 1$; (d) $TR = 0.34$, $CORR = 3$. At the collector inlet, air is at ambient condition but gains heat after interacting with the high- temperature glass surface of the PV module. Subsequently, heated air flows through the flow passage due to buoyancy forces and the updraft generated by the vertical chimney.

Following points are noted from the velocity field: 1. Lowest velocity rise is seen for tapered collector with conventional chimney design (Fig. 3.14(c)), 2. Highest velocity rise is observed for conventional collector design with divergent chimney (Fig. 3.14(b)), 3. Intermediate velocity gain of about 5.5 m/s is seen for tapered collector with divergent chimney. At the face of it, it might seem that the design with highest velocity gain would be best suited for the PV panel integrated solar chimney plant. However, a closer look at the temperature changes of the PV panel suggest a different scenario. The average PV panel efficiency for highest velocity gain case was 4.4% while for system with 5.5 m/s gain, the efficiency was just above 7%. Clearly, higher temperature drop in the PV panel was achieved at the cost of reducing the velocity. The tapering the collector reduced the hydraulic performance, but it increases the thermal performance of the PV panel.

Figure 3.15 air pressure distribution for various designs of HSCPP at collector solar irradiance of 850 W/m2:

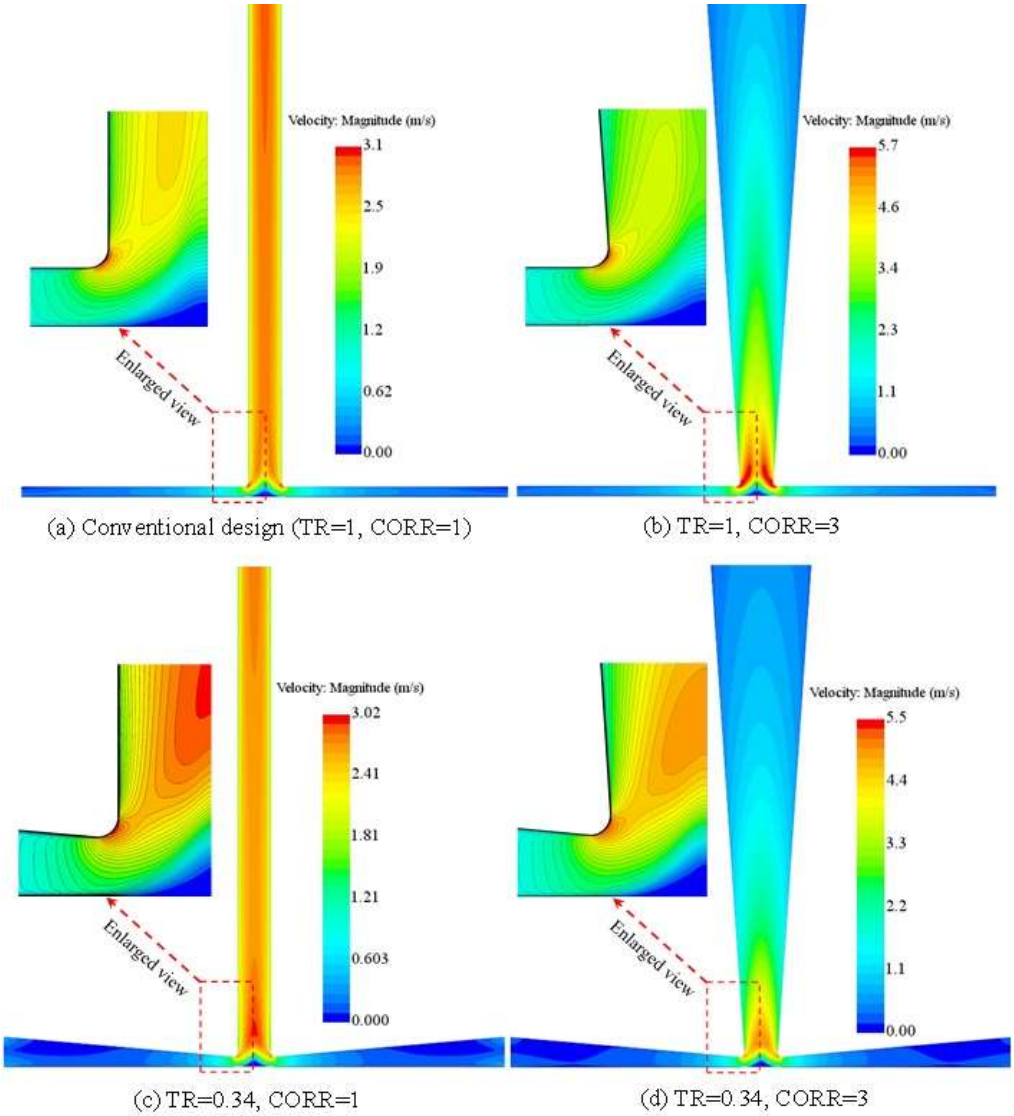

Figure 3.14: Velocity contours for various designs of HSCPP.

Table 3.6: Performance data of various HSCPP designs. Note that $TR = 1$ and $CORR = 1$ represent conventional hybrid solar chimney power plant.

TR	CORR	Velocity at collector exit (m/s)	PV panel % efficiency gain	Static pressure recovery: $\frac{1}{2}\rho({v_1}^2 - {v_2}^2)$ (N/m^2)	Power (W)
1	1	1.80	-	-	0.433
0.83	1	1.84	2.1	-	0.463
0.67	1	1.82	2.6	-	0.448
0.50	1	1.79	3.3	-	0.426
0.34	1	1.78	4.5	-	0.419
1	1.5	2.89	3.2	3.06	1.794
1	2	3.55	4.0	6.56	4.758
1	2.5	3.88	4.2	8.44	4.343
1	3	3.98	4.4	9.28	4.687
1	3.5	3.87	4.3	9.19	4.309
1	4	3.76	4.3	9.13	3.952
1	4.5	3.63	4.1	8.62	3.556
1	5	3.59	3.9	8.00	3.440
0.34 (best)	***3***	***3.12***	***7.1***	***5.60***	***2.258***

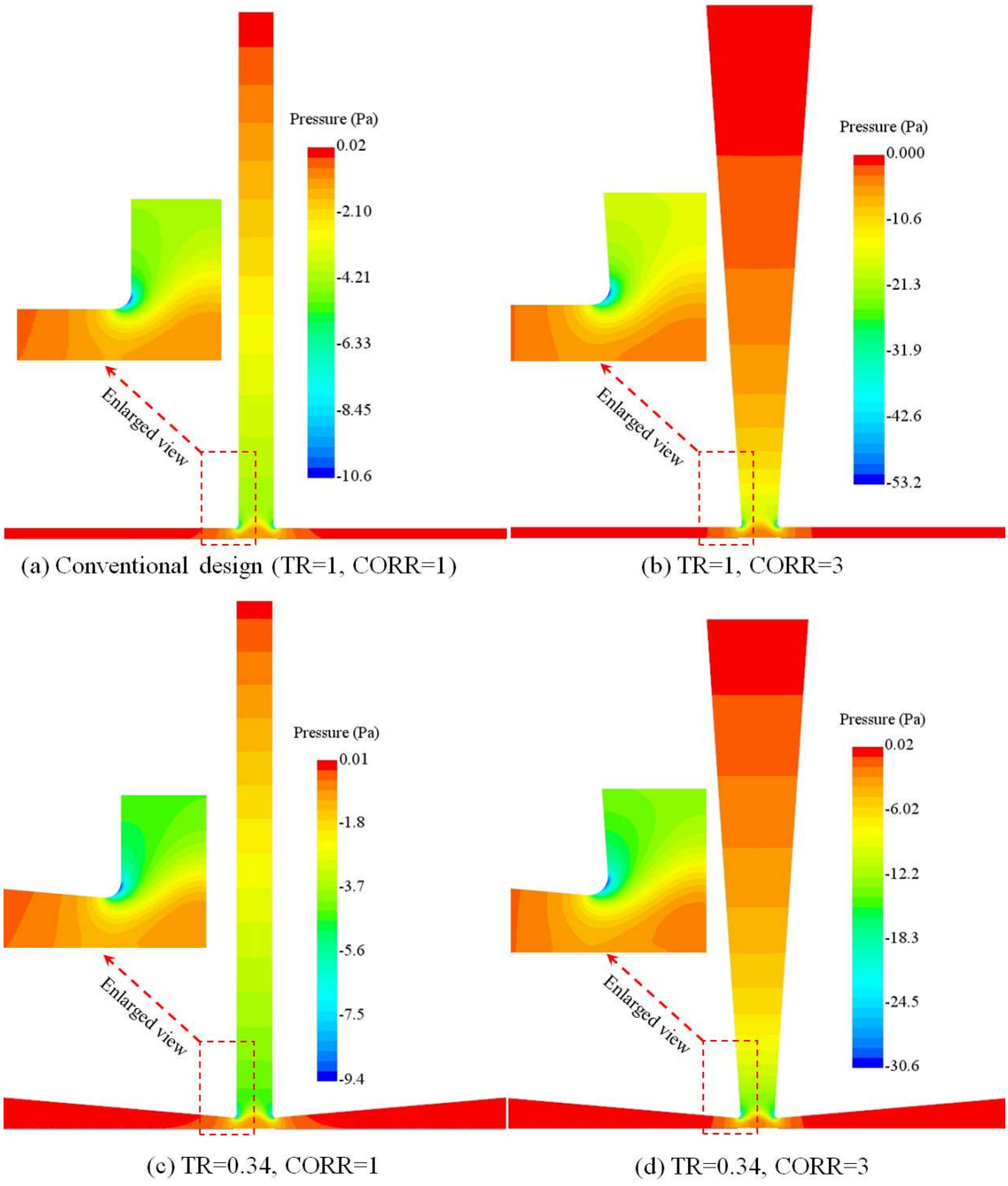

Figure 3.15: Pressure contours for various designs of HSCPP.

(a) conventional ($TR = 1$, $CORR = 3$); (b) $TR = 1$, $CORR = 3$; (c) $TR = 0.34$, $CORR = 1$; (d) $TR = 0.34$, $CORR = 3$. As discussed earlier, the conventional design does not aid in static pressure recovery. Transforming conventional cylindrical chimney design to divergent has a significant impact on the flow field due to static pressure recovery from the dynamic pressure. With increasing CORR values, TPP follows parabolic variation. Total pressure potential shows positive trend up to $CORR = 3$ and thereafter, it starts decreasing due to adverse pressure gradient near the outlet region. The best design configuration is $TR = 0.34$ with $CORR = 3$ for enhancing the PV panel efficiency and turbine power output.

Figure 3.16 shows turbulent kinetic energy (TKE) for various designs of HSCPP. The TKE has maximum value at the chimney inlet and decreases along the chimney height. With increase in mean velocity, TKE also increases and thus, increases the rate of heat transfer in the collector and cooling of the PV panel. As shown in Fig. 3.16, the case (d) with $TR = 0.34$ integrated with divergent chimney with $CORR = 3$ possess maximum TKE value of 2.1 J/kg. This enhances flow mixing near to the collector bottom wall of the PV panel. Higher convection heat transfer results in increase in PV panel efficiency by 7%.

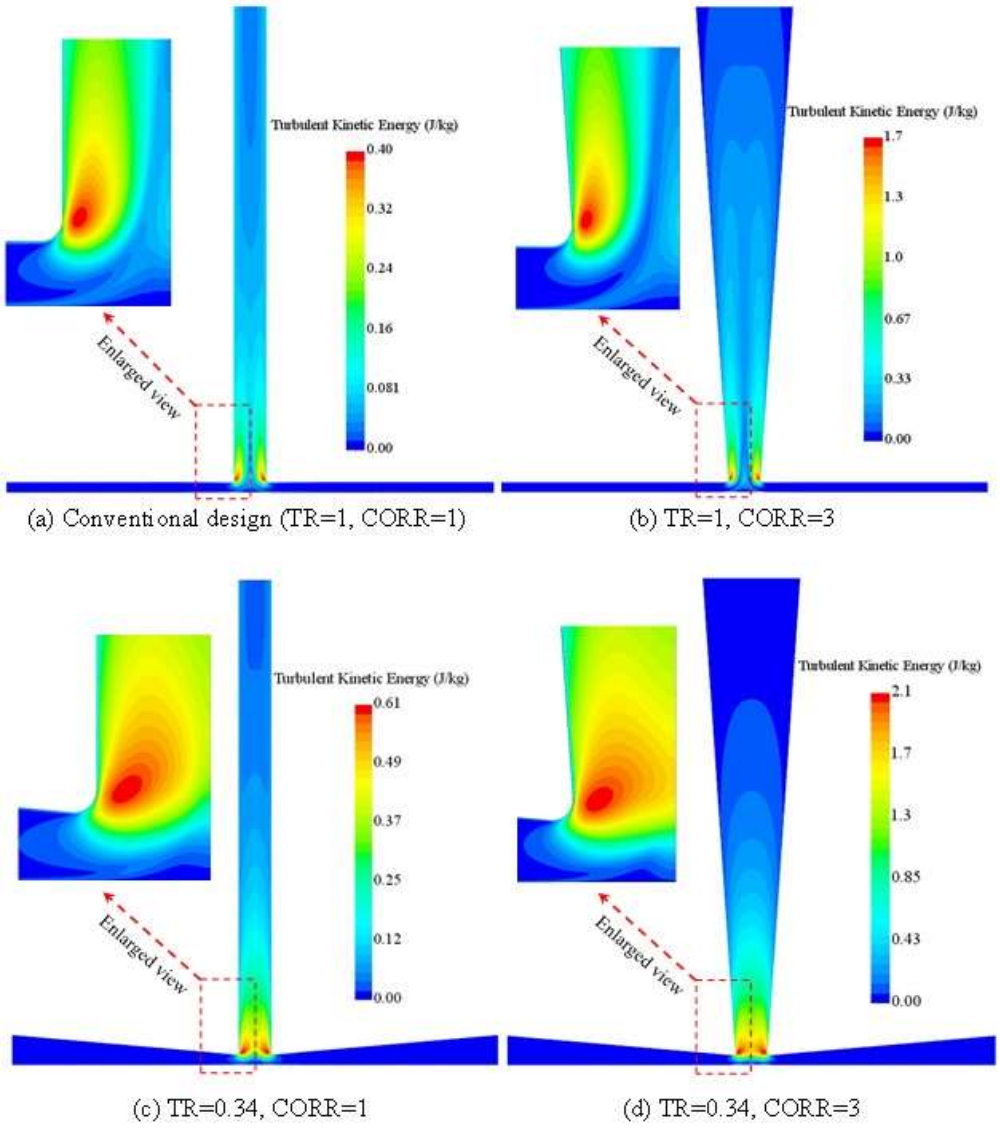

Figure 3.16: Turbulent kinetic energy for various designs of HSCPP.

From the above discussion, it is now clear that PV panel power generation efficiency is considerably affected by design of the solar chimney plant. We now broadly classified the various design configurations investigated in this chapter based on the PV panel efficiency (see Fig. 3.17). Designs investigated here are not exhaustive and there may exist many sub-designs that may fall in between the classifications. It is evident that conventional designs of both collector and chimney has to be modified to achieve higher PV panel efficiency. Future research could involve directed cooling of the PV panel by bleeding cold air near the panel or using some combinations

of air along with other fluids such as water or placing phase change materials beneath the panel.

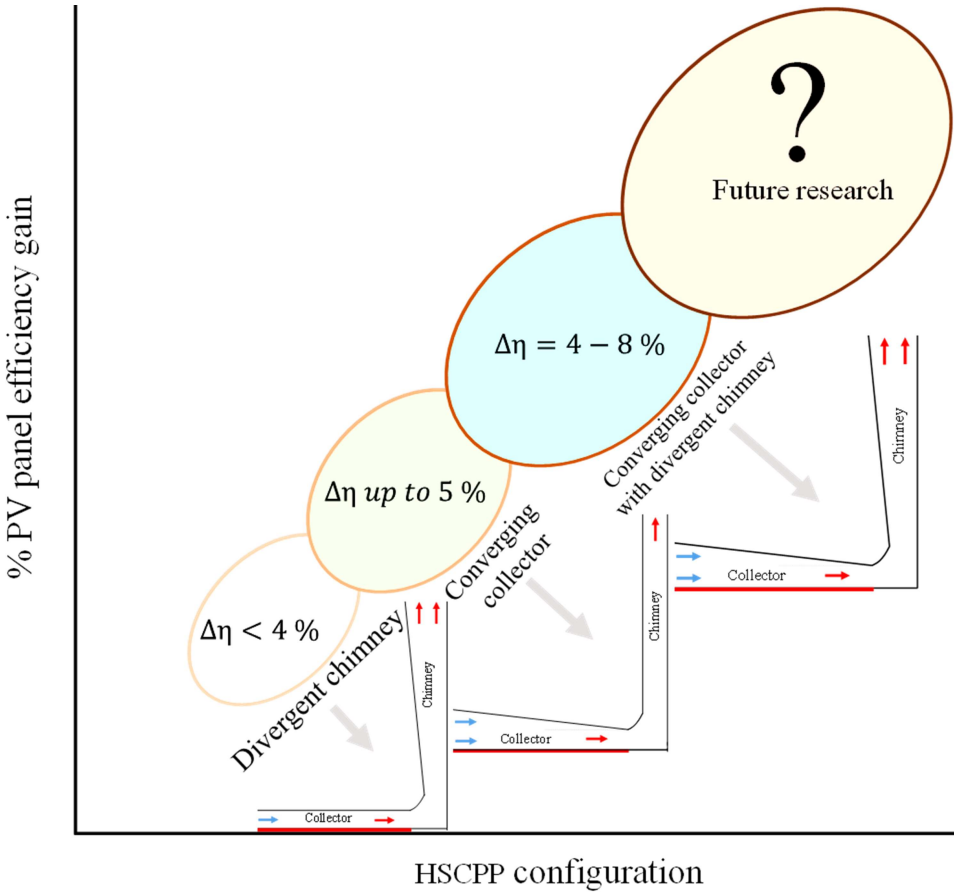

Figure 3.17: HSCPP designs categorization based on percentage gain in photovoltaic electrical conversion efficiency compared to the conventional HSCPP design.

3.5 Conclusion

A 2D axisymmetric numerical model of a hybrid solar chimney power plant integrated with a photovoltaic panel is developed. Since the conventional solar chimney possess very low thermal to electrical conversion efficiency, this chapter explored the avenues of integrating and enhancing the PV panel electrical conversion efficiency in the collector duct. Various design configurations of collector duct and solar chimney was investigated for increasing the PV panel efficiency in terms of temperature drop and turbine power output in terms of air velocity changes in the system. The hybrid system was studied for the range collector taper ratio (TR: $0.34 - 1$) and chimney outlet to inlet radius ratio (CORR: $1 - 5$). Following are the important findings of the research:

1. Initially, increasing the chimney outlet radius enhances the HSCPP performance for CORR $1.5 - 3$. However, further increase in outlet radius deteriorates performance in CORR range $3.5 - 5$. Static pressure recovery was highest for $CORR = 3$. At this value, the flow velocity was considerably enhanced by 121%, and hence the turbine power output by 363%. The PV panel efficiency increased by about 4%.

2. No significant gain in turbine power output was observed by only tapering the collector flow passage. However, PV panel electrical output increased by maximum 4.5% for collector taper ratio 0.34.

3. Results show that neither the divergent chimney nor a tapered collector duct designs alone are sufficient to enhance the system performance when integrated with the PV panel. The combination of suitable design changes in both collector and chimney seems the best design strategy for hybridization of solar chimney system. High electrical efficiency of PV panel was observed (by about 7%) with taper ratio 0.34 and $CORR = 3$.

4. About 80% of the collector area near the chimney is the most influential region for cooling of the PV panel, where consistent temperature drop of $10 - 12°C$ was observed. This manifested an increase in the PV panel electrical output efficiency by about 7%.

5. Design categorization of the solar chimney was presented in terms of percentage gain in PV panel efficiency. To achieve higher efficiency gain beyond 10%, further innovative design changes in the inlet design of collector in combination with other cooling mechanisms such as phase change materials can be investigated.